

# Can a photometric redshift code reliably determine dust extinction?

T.S.R Babbedge<sup>1\*</sup>, R. Whitaker<sup>2†</sup>, S. Morris<sup>2‡</sup>

<sup>1</sup>*Astrophysics Group, Blackett Laboratory, Imperial College London, Prince Consort Road, London SW7 2BW, UK.*

<sup>2</sup>*Astronomy and Astrophysics, Physics Department, South Road, Durham DH1 3LE, UK.*

Accepted 2005 May 04. Received 2005 April 04; in original form 2004 December 21

## ABSTRACT

Photometric redshifts can be routinely obtained to accuracies of better than 0.1 in  $\Delta z/(1+z)$ . However, the issue of dust extinction is one that has still not been well quantified. In this paper the success of two template-fitting photometric redshift codes (IMPZ and HYPERZ) at reliably returning  $A_V$  in addition to redshift is explored. New data on the CNOC2 spectroscopic sample of  $0.2 < z < 0.7$  galaxies are presented. These data allow us to estimate  $A_V$  values from the observed Balmer decrements. We also investigate whether the empirical value of  $\gamma = 0.44$ , the ratio between gas- and star- derived extinction, as determined by Calzetti (2001b), is necessarily the best value for this sample.

When comparing the two codes to the Balmer-derived  $A_V$ , a correlation between the photometrically derived  $A_V$ , Phot- $A_V$ , and the Balmer- $A_V$  is found. The correlation is improved when the empirical value of  $\gamma = 0.44$  is allowed to vary. From least-squares-fitting the minimum in the reduced  $\chi^2$  distribution is found for  $\gamma \sim 0.25 \pm 0.2$ . For the sample of galaxies here, the factor of two difference in covering factor implied by the Calzetti ratio is found to be plausible. The CNOC2 galaxies with detected Balmer lines have some preference for an increased covering factor difference, which would perhaps imply they are undergoing more rapid, ‘bursty’ star formation than the galaxies Calzetti used in her derivation.

**Key words:** galaxies:evolution - galaxies:photometry - quasars:general - cosmology: observations

## 1 INTRODUCTION

Star formation rates (SFRs) and their global history (SFH) form the backbone of a slew of methods (observational, numerical, and analytical) investigating the processes of galaxy formation and evolution over cosmic time. The SFH is important in indicating likely eras of dominant activity and in providing a self-consistent picture of chemical enrichment. This can then be compared to the predictions of semi-analytical models of galaxy formation and with intergalactic medium (IGM) absorption line diagnostics. However, SFRs can be imprecise due to complications arising from dust extinction.

COBE measurements of the cosmic far-IR/sub-mm background energy density (Puget et al. 1996) showed it to be equal to, or greater than, the UV/optical background (e.g. Hauser et al. 1998), implying that a large fraction of the energy from stars over the history of the Universe is hidden in the optical due to dust. The role of dust in high redshift galaxies has been discussed by many authors (e.g. Rowan-Robinson et al. 1997; Pettini et al. 1998; Calzetti & Heckman 1999; Adelberger & Steidel 2000). For example, star forming galaxies detected via the Lyman break technique at  $z \sim 2 - 4$  are estimated to be highly extinguished in the rest-frame UV, meaning star formation rates are  $\sim 3 - 10$  times higher than if dust is ignored (e.g. Meurer, Heckman & Calzetti 1999). Correction factors found for other high redshift star forming galaxies are of a similar order. The exact form of this extinction correction remains uncertain and in particular so does its evolution with epoch.

Hence an important improvement for optical-based

\* Email: tsb1@imperial.ac.uk

† Email: r.j.whitaker@durham.ac.uk

‡ Email: Simon.Morris@durham.ac.uk, Visiting Astronomer, Canada-France-Hawaii Telescope operated by the National Research Council of Canada, the Centre National de la Recherche Scientifique de France and the University of Hawaii.

SFH studies is the determination of the extinction of galaxies, in addition to their redshifts. In order to fully allow for variation from galaxy to galaxy, extinction needs to be measured as an additional free parameter to redshift. However the study of Bolzonella, Miralles & Pelló (2000) found that the inclusion of  $A_V$  as a free parameter in photometric redshift codes caused significant increases in aliasing. In a similar technique developed in Rowan-Robinson (2003), hereafter RR03, and extended in Babbedge et al. (2004), hereafter B04, these aliasing problems were reduced by setting several  $A_V$  priors.

In this paper a sample of galaxies from the Canadian Network for Observational Cosmology (CNOC2) Field Galaxy Redshift Survey (Yee et al. 2000) is used to investigate the reliability of  $A_V$  values as determined by two SED template fitting photometric redshift codes – HYPERZ (Bolzonella et al. 2000) and IMPZ (see B04) – by comparing the returned  $[z_{phot}, A_V]$  to the spectroscopically derived redshifts and Balmer decrement derived  $A_V$ 's as calculated from CFHT MOS spectroscopic data.

In §2 the CNOC2 galaxy sample is set out, along with the follow-up CFHT spectroscopic data and Balmer decrement calculations. In §3 we discuss the link between Balmer extinction and photometry. The photometric redshift method is briefly outlined in §4 and the results of applying the two redshift codes to the CNOC2 sample are presented in §5. Overall discussions and conclusions are presented in §6.

Note that for these investigations the flat,  $\Omega_\Lambda=0.70$  cosmological model with  $H_0=72 \text{ km s}^{-1}\text{Mpc}^{-1}$  is used.

## 2 CNOC2 OVERVIEW

The 2nd Canadian Network for Observational Cosmology Field Galaxy Redshift Survey (CNOC2) was conducted over a series of 53 nights on the Canada-France-Hawaii Telescope from 1995 – 1998 (Yee et al. 2000). The survey covers a total area of 1.5 sq. deg. spread over 4 patches equally spaced in RA. The dataset includes  $\sim 6000$  galaxy spectra with spectroscopic redshifts to a nominal limit of  $R_c \sim 21.5$  in addition to 5-colour ( $I_c, R_c, V, B, U$ )<sup>1</sup> photometry of 40,000 galaxies, complete to  $R_c=23.0$  mag. The mean limiting magnitudes (Vega,  $5\sigma$ ) in each filter for the four areas are given in Table 1 and the filter response curves are shown in Figure 1.

Use of a band-limiting filter restricted the spectral window in the survey to 4400 – 6300Å. This includes the [OII] emission line for redshifts between 0.18 and 0.69. The survey's results on galaxy clustering over this range have been published (Shepherd et al. 2001; Carlberg et al. 2000) whilst an analysis of cosmic star formation history is in preparation (Whitaker et al, in prep.).

### 2.1 Extension of the CNOC2 Survey

In this paper we present follow-up observations of a subset of the CNOC2 sample of galaxies. The goal of the additional

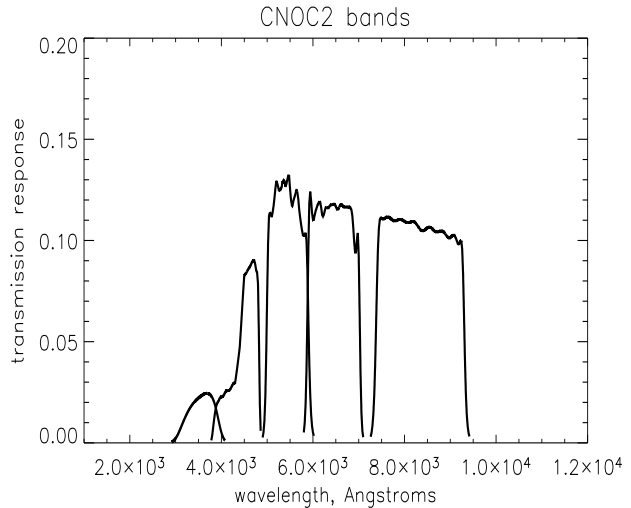


**Figure 1.** CNOC2 passbands combined with CCD response. From short to long wavelength they are U, B, V,  $R_c$ ,  $I_c$ .

**Table 1.** 5-sigma limits (Vega) for the four CNOC2 areas, and the Galactic extinction  $E(B - V)$  in each area. This can be converted to a correction in each band via Cardelli et al. (1989) with  $R_V=3.1$ .

Area	$I_c$	$R_c$	$V$	$B$	$U$	$E(B - V)$
0223	22.97	24.02	23.95	24.55	22.98	0.036
1447	23.52	23.72	24.35	24.76	23.27	0.029
0920	22.85	24.03	23.94	24.55	23.18	0.012
2148	22.69	23.88	23.70	24.48	23.08	0.035

observations was to observe wavelength ranges including the  $H\alpha$  and  $H\beta$  lines in order to set limits on the reddening of the objects and hence to allow estimation of the unreddened star formation rates for this subsample. As will be shown below, this subsample then allows us to test other means of reddening estimation and hence obtain reddening measurements for the entire CNOC2 sample.

In order to maximise the run efficiency, masks were designed with slits assigned as a first priority to objects with  $0.2 < z_{spec} < 0.37$  (allowing observation of both Balmer lines) and detected [OII]  $\lambda 3727$  emission. Second priority was assigned to objects within the same redshift range, but no detected [OII], and third priority to galaxies within the CNOC2 magnitude range which did not yet have redshifts. This last sample will not be used in this paper.

Data was taken with the CFHT MOS spectrograph (Crampton et al. 1992) during a 4 night observing run in August 1999. 17 masks containing a total of 719 slits were observed, spread across 3 of the CNOC2 ‘patches’. The R300 grism was used giving a potential wavelength coverage from 4000-10,000Å (depending on slit location), with a dispersion of 5Å per CCD pixel. A slit width of 1.5'' was used giving a nominal spectral line FWHM of 3.4 pixels or 17Å.

The data were reduced in IRAF (Tody 1993)<sup>2</sup>. The

<sup>1</sup>  $V$  photometry is actually  $g$ -band data calibrated to the  $V$  system based on Landolt standards

<sup>2</sup> IRAF, the Image Reduction and Analysis Facility, is a general

**Table 2.** Windows used for H $\alpha$  and H $\beta$  in this study

Feature	Window ( $\text{\AA}$ )	
	continua	line
H $\alpha$	6490–6536; 6594–6640	6537–6593
H $\beta$	4785–4815; 4911–4931	4821–4901

reduction was based on a slightly modified version of the CNOC2 standard reductions of Yee et al. (2000). The steps included object finding, tracing and extraction, wavelength calibration, flux calibration, and interpolation over bad sky subtraction and zero order residuals. Error vectors were carried through the same procedure.

## 2.2 Measurement of the Balmer Decrement from CNOC2

Our own purpose written code (Whitaker et al., in prep, based on the code by Balogh 1999) was used to measure the fluxes and equivalent widths of the Balmer lines in each spectrum. In brief, the code measures the flux and equivalent width over pre-defined spectral windows, set for each line. Each window includes two continuum regions and a line region. We perform a  $1.5\sigma$  clip on the continuum regions to reject outliers and improve the quality of the continuum fit. Table 2 shows the windows we use for H $\alpha$  and H $\beta$  in this study. We note that our H $\alpha$  definition is similar to that of Balogh et al. (2002) with two minor modifications: Firstly we use a wider line region in order to fully encompass the H $\alpha$ + [NII] flux in our measurement; this necessarily reduces the size of the blue continuum region by  $1\text{\AA}$ . This should have minimal affect on the quality of the continuum fits. The H $\beta$  window we use is identical to that of Dressler & Shecter (1987).

While it is true that the continuum fit is obtained from only 7 (4) independent points for H $\alpha$  (H $\beta$ ), the actual number of data points used in the fit is considerably more: 23 (13) for H $\alpha$  (H $\beta$ ), i.e.  $\sim 3$  data points per resolution element. As a result, any spurious points, from cosmic rays or the like will be safely rejected without substantially reducing the quality of the fit.

Figure 2 shows 3 typical spectra from our sample – the window regions are overplotted.

Error estimates on the equivalent widths are computed using the formulae set out by Bohlin et al. (1983). For the error on the flux measurement we employ the following rule:

$$\sigma_F = F \frac{\sigma_W}{W} \quad (1)$$

where  $F$  and  $W$  signify the measured flux and equivalent width and  $\sigma_F$  and  $\sigma_W$  their respective errors.

purpose software system for the reduction and analysis of astronomical data. It is written and supported by programmers in the Data Products Program of the National Optical Astronomy Observatory, which is operated by the Association of Universities for Research in Astronomy, Inc., under cooperative agreement with the National Science Foundation.

The original CNOC2 dataset contains multiple observations of certain galaxies and using these we are able to assess whether we systematically under- or over-estimate the equivalent width errors. Our procedure is to compute for each pair of repeats a quantity  $\epsilon$  such that:

$$\epsilon = \frac{W_1 - W_2}{(\sigma_1^2 + \sigma_2^2)^{\frac{1}{2}}} \quad (2)$$

Where  $W$  and  $\sigma$  are as in Equation 1; the subscripts 1 and 2 refer to the separate observations. The perfect case is where the distribution of  $\epsilon$  is a unit gaussian of mean zero. This would imply that we have accurately measured the errors and there are no systematic under- or over-estimates.

Such a unit gaussian is not found using the raw errors and so they are scaled according to the following equation.

$$\sigma_{true}^2 = A\sigma_{raw}^2(1 + B(\sigma_{raw}^2 - ave^2)) \quad (3)$$

Where A and B are multiplying factors to be determined and  $ave$  is the average raw [OII] equivalent width error larger than  $2\text{\AA}$ . We recompute the distribution of  $\epsilon$  for a range of A and B and check whether it is a unit gaussian. The process is repeated until a unit gaussian is found.

The same scaling we apply to the [OII] errors is then applied to the H $\alpha$  errors in this work (see Whitaker et al., in prep., or Balogh 1999 for the full details of this procedure).

## 2.3 Correction For [NII] Emission and Stellar Absorption

The window we employ in our spectral measurement code encompasses both the H $\alpha$  and [NII] lines. We cannot separate the two lines in our data, nor are we able to accurately de-blend them using gaussian fitting tools (e.g. *splot* in IRAF) since the data is not of high enough resolution. Instead, to correct for [NII] we assume an [NII]/H $\alpha$  ratio of 0.5 (as per Kennicutt 1992). This is a simple approximation, however a by-eye examination of spectra in our sample reveals that it is not obviously incorrect (see e.g. Figure 2). Using an extreme value for the NII/H $\alpha$  ratio such as 0.33 which Kennicutt & Kent (1983) find for HII regions, results in a difference of  $\sim 0.4$  in  $A_V$  compared to the [NII]/H $\alpha$ =0.5 case. This value for HII regions does not incorporate the effects of interstellar gas with its higher mean [NII]/H $\alpha$  ratio, and since our spectra are from the galaxy as a whole rather than individual HII regions we assume the 0.5 factor to be the most reasonable.

The Balmer emission lines sit on top of stellar absorption due to the presence of young and intermediate age stars in the line-emitting galaxy, so any measurement of their fluxes must take this into account. This is particularly true for H $\beta$ , where one often finds an emission line sitting in an absorption trough (see the middle right-hand panel of Figure 2 for an example of this).

Again, due to the restrictions imposed by the data, we are not able to reliably fit the emission and absorption components separately within each line, so instead choose to apply the corrections used by the Sloan Digital Sky Survey (SDSS: Hopkins et al. 2003). They measure a median absorption at H $\alpha$  of  $2.6\text{\AA}$  (note we do not employ their correction of  $1.3\text{\AA}$  since we are using a window measurement method to obtain our fluxes, not the gaussian fits of the SDSS pipeline). For the H $\beta$  correction, we use the value for

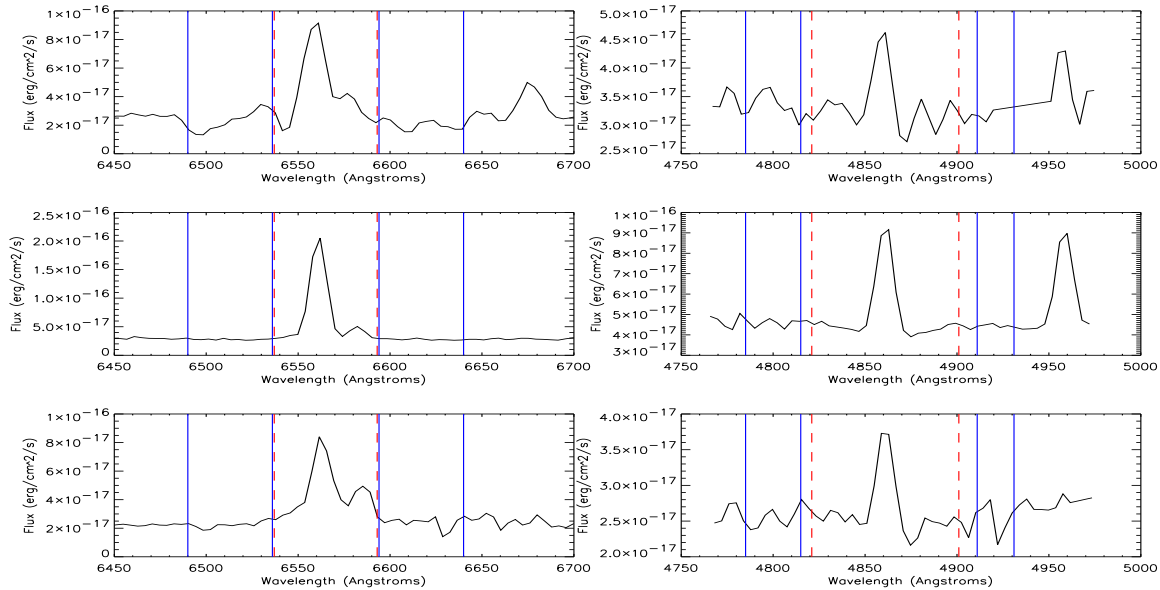


**Figure 2.** Three typical spectra from which we measure the Balmer decrement. **Left column** shows the  $H\alpha$  region, the **right column** shows the  $H\beta$ . The window regions are overplotted: the solid (blue) lines show the continua regions, the dashed (red) lines the line region. The spectra are shown in rest-frame wavelength, the mean redshift of the whole sample is  $\sim 0.286$

Sb Galaxies ( $2\text{\AA}$ ) given by Miller & Owen (2002), also used by the SDSS.

In addition to the above two corrections to the flux measurements we also do the following: For sources with a secure  $H\alpha$  detection but either a low significance  $H\beta$  detection in emission, or detection at any significance level of  $H\beta$  in absorption, we reset the  $H\beta$  flux to be its  $3\sigma$  error value. For the emission cases this is an obvious step, for the absorption cases however, it should be stated that the maximum  $H\beta$  emission flux is still the  $3\sigma$  value – the absorption may of course be larger than this, but since the galaxies are emitting at  $H\alpha$ , they must therefore be emitting at  $H\beta$  also.

Figures 3 and 4 show the flux distribution of  $H\alpha$  and  $H\beta$  both before and after the above corrections for [NII] and stellar absorption. In figure 4 the reset  $H\beta$  values are plotted as arrows, indicating an upper limit on the flux.

## 2.4 Balmer Line Detections and Limits

We divide the 719 objects observed in the extension to the CNOC2 dataset as follows:

- 367 objects do not have redshifts in the original CNOC2 survey and so are removed from our sample.
- Of the remaining 352 objects, 46 are removed, either due to skylines obscuring the  $H\beta$  line (33 objects), or problems with the noise measurements arising from the data reduction procedures (13 objects).

This leaves 306 objects, and of this subset:

- 46 objects possess both emission lines measurable at above  $3\sigma$  accuracy (we refer to these as ‘measure’ cases).
- 153 objects have only  $H\alpha$  measurable to an accuracy above  $3\sigma$  –  $H\beta$  is not measurable to such accuracy in these spectra (we refer to these as ‘limit’ cases, i.e. we obtain a lower limit to the reddening for these objects).

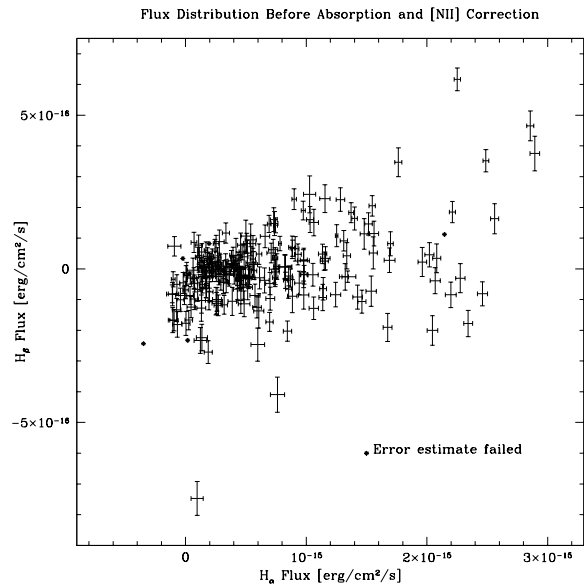


**Figure 3.** The flux distribution of  $H\alpha$  and  $H\beta$  prior to corrections for [NII] and stellar absorption.

- 107 objects have neither  $H\alpha$  or  $H\beta$  emission detectable at above  $3\sigma$  accuracy, thus we are unable to estimate a lower limit on the reddening from these galaxies.

Of the set of 46 measurements, five of them fall  $> 3\sigma$  below zero and of these five, four are removed (see below). This leaves 42 measured sources for the analyses carried out later in this paper. We note that in a large enough sample, some objects are expected to lie  $3\sigma$  below zero reddening,

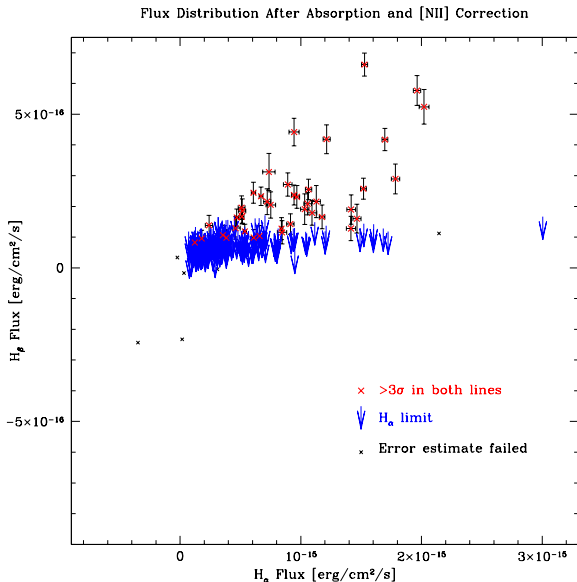


**Figure 4.** The flux distribution of  $H\alpha$  and  $H\beta$  after corrections for [NII] and stellar absorption. Crosses are sources with a detection of at least  $3\sigma$  in both  $H\alpha$  and  $H\beta$ , arrows denote sources with an  $H\alpha$  detection of at least  $3\sigma$  but where the  $H\beta$  flux has been reset to a  $3\sigma$  limiting value. Sources in which neither line could be measured at above  $3\sigma$  are not plotted.

due to the nature of the statistics. We now describe the five objects in question:

- Three objects appear to be blends where two (or more) galaxies are co-extracted from the slit; it is impossible to derive a reddening measurement from these spectra.
- One object has an error in the noise vector.
- One object has a high quality spectrum but a relatively small [NII] flux. Our methodology of using a coarse correction for the [NII] flux serves to push extra objects into the  $3\sigma$ -below-zero reddening range (in addition to those we naturally expect from gaussian statistics). This object is retained in the sample.

Of the set of 153 lower limit cases we note that 70 produce limits below zero reddening. Again, given our error approach, this is not surprising.

The mean redshift of the sample of ‘limits’ and ‘measures’ (Figure 4) is  $\sim 0.262$  while that of every object (Figure 3) is  $\sim 0.286$ .

## 2.5 Selection Effects

The ‘measures’ sample we define and use in this work is subject to certain selection effects.

The observations are clearly most sensitive to galaxies which have strong emission lines and low to moderate  $A_V$ . Any galaxies with weak emission lines and moderate  $A_V$  will be lost from our sample since the lines will have been diminished to the extent where they are undetectable. This is also true for galaxies with large extinction – at least  $H\beta$ , if not both Balmer lines, will have been diminished by too great an amount to be detectable. The best that can be accom-

plished in that case is to estimate a limit on the extinction, as we have done here.

The problem of skyline contamination of the  $H\beta$  line is one which all projects attempting reddening measurements in external galaxies will suffer from. However this will not affect our results unless there exists a strong correlation of extinction with redshift such that certain extinctions occur at certain redshifts where the  $H\beta$  line is obscured. Given the narrow redshift range of the survey and the strength of correlation that would be required this is not anticipated to be an issue.

## 2.6 Calculation of extinction from the Balmer ratio

The  $H\alpha$  and  $H\beta$  Balmer lines provide a probe of extinction for the optical region of the spectrum – their un-extincted intensity ratio is well known from atomic physics (Osterbrock 1989) and is 2.86 in typical nebula conditions ( $T=10,000\text{K}$ ,  $n_e = 10^2 - 10^4\text{cm}^{-3}$ ). Their ratio thus leads to the Balmer optical depth,  $\tau$ , and can therefore provide a measure of the dust content due to the internal reddening along the line of sight (e.g Calzetti et al. 1994), down to an optical depth of  $\tau \sim 1$ .

The observed ratio,  $R_{obs}$ , of  $H\alpha/H\beta$  can be shown to be related to the reddening to the gas,  $E(B - V)_g$ , according to the following equation (e.g Calzetti et al. 1996):

$$E(B - V)_g = \frac{2.5[\log(R_{obs}) - \log(R_{int})]}{k(H\beta) - k(H\alpha)} \quad (4)$$

where  $R_{int}$  is the intrinsic  $H\alpha/H\beta$  ratio of 2.86 and  $k(H\alpha)$  and  $k(H\beta)$  are the extinction coefficients at the wavelengths of  $H\alpha$  and  $H\beta$  respectively (from Calzetti et al. 1993).

The Calzetti curve (Calzetti et al. 1993) was used to compute  $A_V$ 's from the Balmer decrement, with the lowest measured  $A_V$  being -2.25 (this is the source previously mentioned that has low [NII] flux) and the highest 5.15. These values are typically accurate to 30%; the mean of the ratio ( $A_V/\sigma A_V$ ) is 0.27. Figure 5 shows histograms of the 42 Balmer-measured  $A_V$  values as well as the 153 limit cases.

The choice of extinction curve is one of the sources of uncertainty - the extinction curves of local galaxies do differ (e.g see review by Calzetti 2001a). The largest differences are due to the strength of the feature at  $\sim 2175\text{\AA}$ , thought to result from graphite grains, amorphous carbon or PAH. However, for the Balmer lines, this feature is not a factor: The Balmer lines are sampling the longer wavelength region where the extinction curves have a more constant slope, so that differences are reduced. The main difference between the curves here can be parameterised by the chosen value of the ratio  $R_V$ , which is the total-to-selective extinction ratio at V band (Calzetti et al. 1993). In these investigations  $R_V=4.05$  is used.

## 3 BALMER EXTINCTION VS. PHOTOMETRY

Are we able to compare photometry-derived extinction values, hereafter Phot- $A_V$ , to Balmer- $A_V$  values in order to better understand the accuracy and/or reliability of photometry-derived extinction measurements?

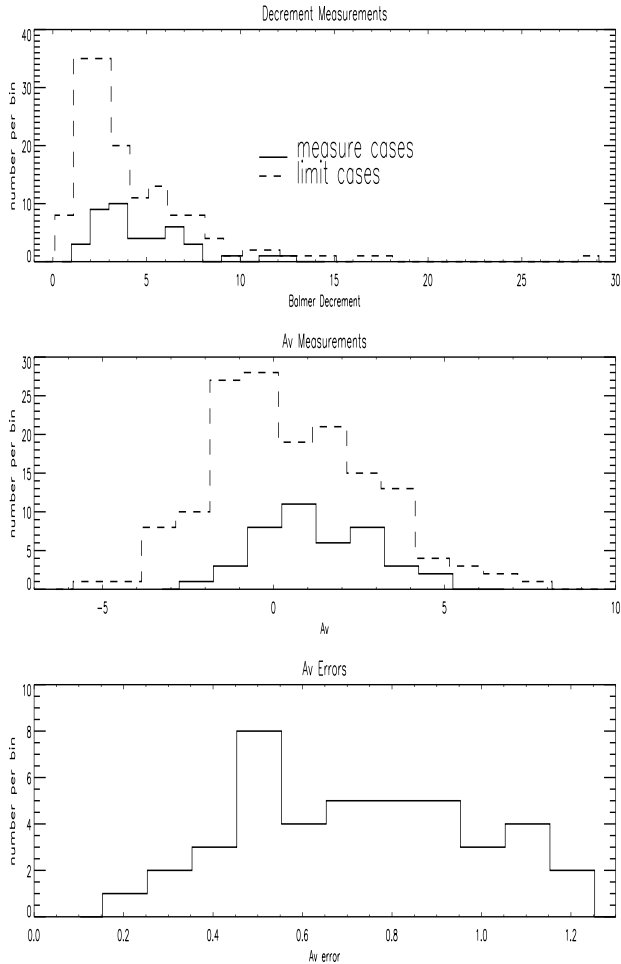


**Figure 5.** The distribution of Balmer decrements (top panel), Balmer-derived  $A_V$  values (middle panel) and associated error (bottom panel). The solid line shows results for the sources measured at above  $3\sigma$  accuracy, the dashed line the limit cases (in this case the decrements and Balmer-derived  $A_V$  values are lower limits).

The crucial point here is that the Balmer decrement probes the extinction  $A_V$  of the ionised gas in the source – the extinction of molecular clouds/HII regions (star-forming regions),  $E(B - V)_g$ . In the SED template-fitting method where photometry in a number of bands is compared to a library of templates with variable internal  $A_V$ , the resulting best-fit returns a template type, redshift and  $A_V$ . In this case the extinction is due to the ISM acting on the stellar continua within the galaxy as a whole. Thus Phot- $A_V$  probes the dust obscuration of the stellar continuum,  $E(B - V)_s$ . This is more complicated than just the total amount of dust between the observer and the source, as would be the case for a single star, as folded into this is information on scattering and the geometrical distribution of dust within the galaxy.

Since the Balmer and photometry methods are probing different regimes of the galaxy extinction, they might well be expected to give differing results. In a galaxy such as starburst where there is a significant amount of heavily-obscured star formation the two regimes will be linked - the galaxy’s overall emission is dominated by the young star for-

mation. At the opposite end of the scale an elliptical galaxy will have little dust or ongoing SFR. In this case the two measures are un-correlated (though both measures are likely to be low). For intermediate-type galaxies the relationship falls somewhere between these two regimes.

The following relationship between the colour excess of the stellar continuum and of the nebular emission lines is given in Calzetti (2001b) and Calzetti (1997) and is as follows:

$$E(B - V)_s = (0.44 \pm 0.03)E(B - V)_g \quad (5)$$

This follows on from Calzetti et al. (1994) where 39 starburst and blue compact galaxies were used to derive an *effective* extinction law. From this, it was found that the difference between the optical depth to the Balmer lines, and to the underlying stellar continuum at the lines was approximately a factor two. Calzetti’s relationship is a purely empirical one but it has often, in the past, been assumed to yield the most appropriate reddening corrections for the integrated light of extended star-forming regions or galaxies (e.g Calzetti et al. 2000; Westera et al. 2004). Here we start with this ratio of 0.44 but then consider other possible values in order to see how the results are affected.

## 4 PHOTO-Z METHODOLOGY

The main outcome of applying a redshift code is the best-fitting redshift, extinction and template SED of each source. In the template-fitting procedure, the observed galaxy magnitudes are converted for each  $i^{th}$  photometric band into an apparent flux,  $f_i^{obs}$ . The observed fluxes can then be compared to a library of template (T) fluxes,  $f_i^{templ}(z, T, A_V)$ , as calculated by convolving the template SEDs with the filter response functions. The reduced  $\chi^2$ ,  $\chi_{red}^2$ , is computed for each point in the hyper-cube of redshift/template/ $A_V$  flux values and the best-fitting solution is selected.

### 4.1 The templates

Here, we use six galaxy templates, presented in B04; E, Sab, Sbc, Scd, Sdm and starburst galaxies. These were generated via spectrophotometric synthesis (see Berta et al. 2004 for more on this procedure) of several Simple Stellar Populations (SSPs), each weighted by a different SFR and extinguished by a different amount of dust, and were designed to reproduce in more detail the empirical low-resolution templates of RR03. These SSPs have been computed with a Salpeter Initial Mass Function (IMF) between 0.15 and 120 solar masses, adopting the Pickles (1998) spectral atlas and extending its atmospheres outside its original range of wavelengths with Kurucz (1993) models from 1000Å to 50,000Å, as described in Bressan, Granato & Silva (1998). Nebular emission is added by means of case B HII region models computed through the ionisation code CLOUDY of Ferland et al. (1998). The adopted metallicity is solar. In addition to the galaxy templates, two AGN templates can be considered. However, for the CNOC2 sample used here it was found that the AGN templates did not provide the best fit to any of the sources, (as expected based on their spectra) so in this paper only the six galaxy templates are considered - they are plotted in Figure 6.

One important consideration for the investigations here, and template-fitting codes in general, is that the extinction output by the photometric redshift codes refer to the  $A_V$  values of the best-fitting solutions. However, these values are those of the variable  $A_V$  which has been *added* to the template in question. In addition to this there is also the issue of the *inherent*  $A_V$  of the templates. This is problematic in that the templates originate from empirical templates drawn from observations, along with alterations found to optimise redshift solutions in previous studies. Their re-generation via spectrophotometric synthesis where the overall template is re-produced using a small number of simple stellar populations (SSPs) is designed to give some insight into the underlying physics of each template. Hence an overall  $A_V$  can be defined, based on the  $A_V$ 's of the contributing SSPs.

In B04 these inherent  $A_V$  values were given (ranging from 0 for the elliptical to 0.74 for the starburst). However it is possible to reproduce the same<sup>3</sup> overall template using different proportions of SSPs with differing  $A_V$  contributions. For example, the starburst template can be generated from young SSPs to give the ‘same’ overall template, but with a total  $A_V$  of either 0.05 or 0.74. Similarly, the Scd can be generated with an  $A_V$  of 1.6 or 0.27. Clearly, then, we should not take the inherent  $A_V$ 's of the SSP solutions at face value (we note that in the case of fitting SSPs to spectroscopic data most of these degeneracies can be expected to be broken). Empirically, we would expect the inherent  $A_V$  of the late-type galaxies (Sab, Sbc, Scd, Sdm) to have an extinction to the gas of perhaps  $A_V \sim 0.5 - 1.0$ , and starbursts to be more dusty ( $A_V > 1.0$ , say).

These SSP degeneracies would imply, then, that photometric data is not able to constrain the extinction to an accuracy of less than perhaps  $\pm 1$  in  $A_V$ . If this is the case, then one would not expect a correlation to be found between the Phot- $A_V$  solutions and the Balmer-derived  $A_V$  even if the two methods were probing the extinction to the same regions of the galaxy. The results in §5 will show that this is overly pessimistic, thus implying that SSP fitting considers more possible combinations than actually occur - there are additional constraints imposed in reality due to the nature of star formation, fueling and feedback that such fits do not incorporate. Since the details of inherent  $A_V$  are undetermined, inclusion in the analysis would introduce an additional free parameter. For this relatively small sample there is insufficient data to properly constrain this so here it is merely noted that inherent  $A_V$  is an additional complication and that it is expected to act to increase the Phot- $A_V$  estimates. If the issue of inherent  $A_V$  is a large one then we will expect it to swamp any Phot- $A_V$ /Balmer- $A_V$  correlation - §5 will show that, in practice, this is not the case.

## 4.2 The IMPZ code

This code was presented in B04. At high redshift, Massarotti, Iovino & Buzzoni (2001) have shown that correct treatment of internal (to the galaxy) dust reddening (the Interstellar Medium) and IGM attenuation (between

the galaxy and observer) are the main factors in photometric redshift success. The effect of internal dust reddening for each galaxy is alterable via fitting for  $A_V$ , using the reddening curve of Savage & Mathis (1979), and the effects of the IGM are incorporated as in Madau et al. (1996). Observed fluxes are compared to template fluxes for  $0.01 \leq \log_{10}(1+z) \leq 0.90$ , equivalent to  $0.02 < z \leq 6.94$ .

Galactic extinction in the CNOC2 regions is low; using the extinction–wavelength relation in Cardelli et al. (1989) we can calculate Galactic extinction in each of the CNOC2 bandpasses and correct for it (see Table 1), though the resulting corrections are negligible.

For the CNOC2 sample survey the following parameters were used, adapted from investigations presented in B04:

Templates: The six galaxy templates (E, Sab, Sbc, Scd, Sdm and Starburst), with IGM treatment and Galactic extinction corrections.

Internal extinction:  $A_V$  limits of -0.3 to 3.0 in the  $A_V$  freedom. Negative  $A_V$  was allowed since the inherent  $A_V$  of the templates is non-zero. For the elliptical template  $A_V$  can take the value zero only, since ellipticals are not expected to have significant internal extinction.

Magnitude limits: B04 found it necessary to apply redshift-dependent absolute magnitude limits to exclude unphysical solutions (such as super-luminous sources at high redshift). Here, the same limits are used: Absolute magnitude limits of  $[-22.5 - 2\log_{10}(1+z)] < M_B < -13.5$  for galaxies.

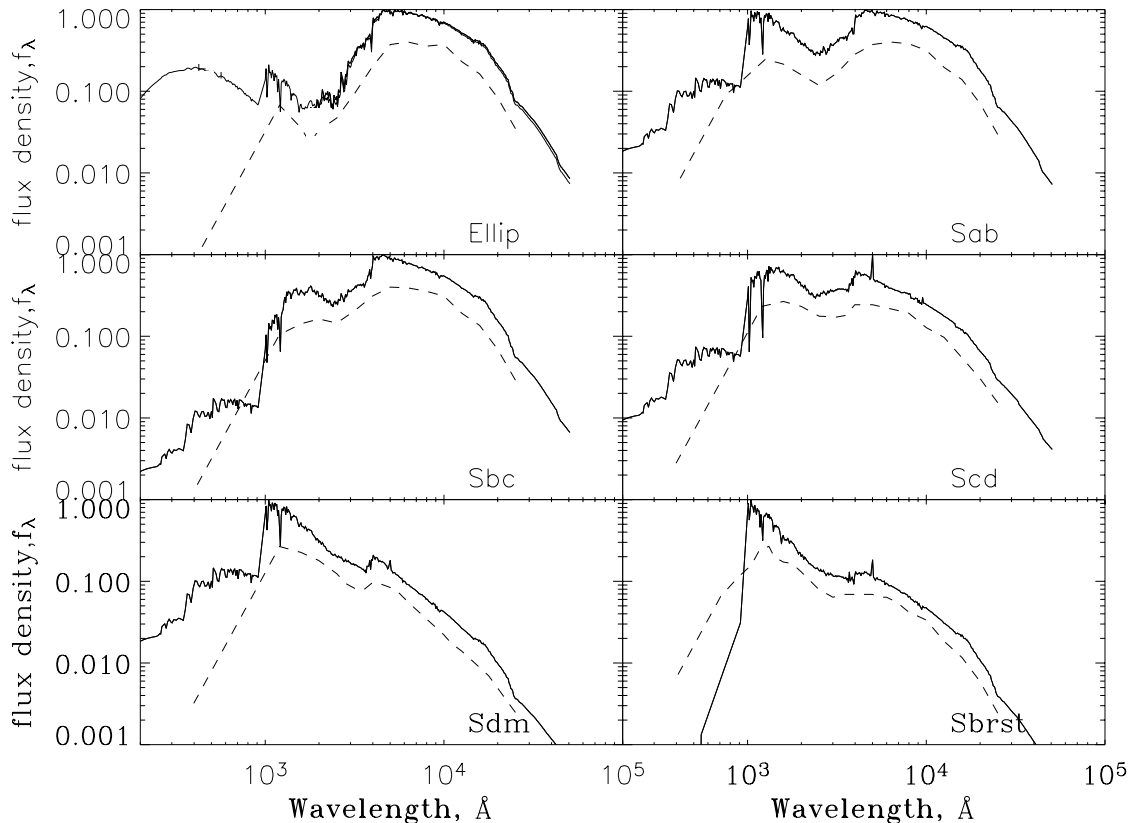
Prior: IMPZ usually applies a prior expectation that the probability of a given value of  $A_V$  declines as  $|A_V|$  moves away from 0. This is introduced by minimising  $\chi_{red}^2 + \alpha A_V^2$  rather than  $\chi^2$  ( $\alpha=2$  here). This use of a prior can be viewed as a weak implementation of Bayesian methods and was reached at based on degeneracy studies in B04 and RR03. For this investigation it was of interest to turn off this prior. This is because the Balmer- $A_V$  values of the sample range from -2.25 to 5.15, or for the starlight (multiplying by 0.44) -1 to 2.3. Hence applying an  $A_V$  prior would naturally tend to limit the  $A_V$  solutions to values in a similar range, regardless of the input  $A_V$  limits, and so some correlation could be achieved simply because the sample all have Balmer- $A_V$  values that equate to the lower end of the  $A_V$  parameter space.

Table 3 shows the parameters used in the final setup for IMPZ and HYPERZ.

## 4.3 HYPERZ

HYPERZ is described in full in Bolzonella et al. (2000). Here we present an overview of the code and the parameters we used for each run. The HYPERZ code also uses SED fitting in its determination of photometric redshifts and for this work we chose to use the same templates as IMPZ. However, for the investigations presented here, we choose to apply HYPERZ for a ‘best-case’ scenario where both the redshift and template type is constrained in order to optimise the resulting accuracy of the extinction values. In order to create such a ‘best-case’ scenario, we choose to remove one degree of freedom by constraining the photometric redshift solution to within ( $z_{spec}/100$ ) of the known spectroscopic redshift. Additionally, we choose not to use the elliptical template in the analysis presented since none of the galax-

<sup>3</sup> here, ‘same’ means from the point of view of flux through a set of broad-band filters



**Figure 6.** The 6 galaxy templates used. Dashed lines show the original RR03 templates (offset for clarity), solid lines shows the SSP generated versions, along with extension into the Far-UV (sub-1000Å) as discussed in B04.

ies with detected Balmer lines are ellipticals based on visual inspection of the spectra.

We do not correct for Galactic extinction when running HYPERZ. This correction is negligible in comparison to the photometric errors (see Table 1 for extinction across the CNOC2 patches) and would not affect the results. Any non-detections in a given band were replaced with a flux of zero, the error being the limiting flux in the band (see Table 1 for  $5\sigma$  limits). Ideally, one would want to provide the measured flux in an aperture placed at the location of the object even when that measurement is fainter than the nominal flux-limit of the survey and the resulting value has very poor S:N. However, the CNOC2 catalogue used here has had such measurements replaced by a ‘non-detection’ flag. Thus the best treatment in the template-fitting procedure is to restrict solutions to those that predict the flux in the non-detected band to be at or below the flux limit in that band.

The HYPERZ code was run in its standard form, with the flat,  $\Omega_\Lambda=0.70$  cosmological model with  $H_0=72\text{km s}^{-1}\text{Mpc}^{-1}$  used elsewhere in this paper and variable  $A_V$  in the range  $0 < A_V < 3$ . Table 3 shows the parameters used in the final setup for IMPZ and HYPERZ.

## 5 RESULTS

### 5.1 IMPZ redshifts

First, it is of interest to see how successful the photometric redshifts are when there is no  $A_V$  freedom - that is,  $A_V=0$  in the solutions. The results of this are plotted in the left panel of Figure 7, for ‘measure’ cases (black squares) and ‘limit’ cases (red crosses). It is immediately clear that not allowing  $A_V$  freedom has caused many of the IMPZ solutions to be incorrect - the code has been forced to substitute (incorrectly) additional redshift in place of the reddening action of dust. Indeed, there are a total of 11 of the 42 ‘measure’ and 70 of the 153 ‘limit’ sources (48% of the sample) whose photometric redshifts lie outside the  $\log(1+z_{\text{spec}}) \pm 0.1$  boundaries.

If we now run IMPZ in the optimal manner, as discussed in §4.2, so that now  $A_V$  freedom is allowed, the solutions dramatically improve. IMPZ was highly successful at deriving photometric redshifts in close agreement with the spectroscopic values for 40 of the 42 ‘measure’ and 147 of the 153 ‘limit’ sources (95% of the sample). Note we consider redshift solutions in the range  $[0:7]$ . There were 8 (2 ‘measure’ and 6 ‘limit’) sources that obtained solutions at incorrect redshifts due to degeneracies in  $[z, \text{template}, A_V]$  space. We measure the accuracy of the photometric redshifts via the *rms* scatter  $\sigma_z$ , calculated as follows:

$$\sigma_z^2 = \sum \left( \frac{z_{\text{phot}} - z_{\text{spec}}}{1 + z_{\text{spec}}} \right)^2 / N \quad (6)$$



**Table 3.** Final parameters for the two photometric redshift codes.

	IMPZ	HYPERZ
Templates	E, Sab, Sbc, Scd, Sdm, Sb	Sab, Sbc, Scd, Sdm, Sb
$M_B$ limits	$[-22.5-2\log_{10}(1+z)] < M_B < -13.5$	not constrained (but set by $z_{spec}$ )
$A_v$ limits, $A_v$ step	$-0.3 \leq A_v \leq 3.0$ , step 0.1	$0.0 \leq A_v \leq 3.0$ , step 0.27
Reddening law	Cardelli 1989	Calzetti 2000
Galactic extinction correction?	Yes	No
Constrained to $z_{spec}$ ?	One run unconstrained, one run constrained	Yes
Cosmology	$\Omega_0=1, \Omega_\Lambda=0.70, H_0=72\text{km s}^{-1}\text{Mpc}^{-1}$	$\Omega_0=1, \Omega_\Lambda=0.70, H_0=72\text{km s}^{-1}\text{Mpc}^{-1}$

with N being the number of sources with both spectroscopic redshifts and photometric redshifts. For this data, the  $rms$ ,  $\sigma_z=0.32$  when including the 8 outliers, or 0.07 when they are excluded. The comparison of spectroscopic and IMPZ redshifts is plotted in the middle panel of Figure 7.

IMPZ is therefore successful at returning accurate redshifts. However, can it also provide a measure of the extinction compatible with that implied by the Balmer decrement? Since 2 of the 42 ‘measure’ sources obtain an incorrect photometric redshift this also means their extinction values are likely to be incorrect. In order to remove this (small) source of error in the following comparisons to the Balmer-derived extinction, we now constrain the redshift range explored by IMPZ to lie within 0.05 in  $\log(1+z_{phot})$  of  $z_{spec}$  (plotted in the right panel of Figure 7). Now, good solutions are found for all 42 ‘measure’ cases and 153 ‘limit’ cases, with  $\sigma_z=0.06$ . It is the resulting IMPZ  $A_V$  values from this setup that are considered from now on in the investigation.

### 5.2 Range of IMPZ $A_V$ allowed values

Although we wish to explore the accuracy of the extinction output from redshift codes by comparing to a sample with Balmer-derived measurements, we can also obtain an internal estimate of how well constrained the  $[z, \text{template}, A_V]$  solution is from the reduced  $\chi^2$  distribution. For the solution with the minimum  $\chi^2$ ,  $\chi^2_{min}$ , the question can be asked: ‘What range of  $A_V$  produces a fit at or near the correct redshift (within 0.05 of  $\log[1+z_{spec}]$ ), with a reduced  $\chi^2$  within  $\chi^2_{min}+1$ ?’

The results of asking this question of each source is illustrated in Figure 8. It can be seen that for the majority of ‘measure’ cases (black), the  $A_V$  is quite well constrained, in most cases to within 0.3 or so in  $A_V$ . Note that the lines in this plot can be discontinuous - for example, object 150 in the plot has a best-fitting  $A_V$  of 1.9 but has reasonable solutions in the  $A_V$  range -0.3 to 0.4 and 0.8 to 1.1 which arise from fitting two other templates to the source. It is of interest to note that whereas 57% of ‘measure’ cases do not have discontinuous solutions, this is only true for 43% of the ‘limit’ (cyan) cases. Thus, determining the  $A_V$  via photometry for these sources is more problematic, just as it is via the Balmer ratio method. Considering the ‘measure’ cases in more detail, there are two objects where the  $A_V$  is poorly constrained (objects 83 and 159 in the Figure, evidenced by their long black lines). Their best-fitting  $A_V$  values are, respectively, 2.3 and 1.7, making them the most heavily extinguished of the IMPZ ‘measure’ cases. Comparison to their Balmer-derived  $A_V$  ( $3 \pm 1$  and  $-1.6 \pm 0.5$  respec-

tively) would support the result for the first source but the Balmer decrement for the second source would imply negative, or zero extinction, disfavoured the IMPZ best-fitting result or resulting in the interpretation that this source is problematic.

Figure 9 illustrates the width of  $A_V$  parameter space that lies within +1 of  $\chi^2_{min}$  by plotting the distribution of this ‘width’ value (here the ‘width’ is simply defined as the maximum allowed  $A_V$  minus the minimum allowed  $A_V$ ). For ‘measure’ cases (black) the distribution drops quite steeply with width such that more than half the sources have a width of 0.4 or less. There is then a slight tail made up primarily of sources which had discontinuous solutions (such as one template with low  $A_V$  and another template with higher  $A_V$ ) whilst the two sources with poorly constrained  $A_V$  can be seen as a spike towards the maximum width of 3.3 (i.e the full -0.3 to 3  $A_V$  range). The distribution for the ‘limit’ cases is more clearly bimodal, with a similar set of reasonably well-constrained sources with an  $A_V$ -width of 0.4 or less, but a much larger set of sources with poorly constrained  $A_V$ . Again, this is likely to be due to the nature of these ‘limit’ sources for whom the dust extinction is hard to determine (either via the Balmer lines or photometry).

This analysis suggests that the photometric redshift solution has an inherently low extinction precision (at least with five band photometry), such that  $A_V$  is only precise to perhaps 0.3 for most sources, and is poorly constrained for a small subset. Rather than defining this internally estimated width value as the error in the Phot- $A_V$  value we choose instead to take the opposite approach for the comparison with the Balmer-derived  $A_V$ . We will take the Phot- $A_V$  at face value and use the supposed relation to the Balmer-derived  $A_V$  to provide an external estimate of the precision of the Phot- $A_V$  measurements.

### 5.3 IMPZ - comparison to Balmer

We can test how well the Calzetti ratio holds by comparing the Phot- $A_V$  to  $0.44 * \text{Balmer-}A_V$ . The distribution of  $A_V$  residuals for IMPZ is plotted in Figure 10. It can be seen that there is quite a spread to the distribution, though it is broadly centred on zero. Based on the findings in §5.2 on the precision of the Phot- $A_V$  solutions some of this spread can be expected to arise from this low precision. Some of it can also be attributed to the accuracy of the Balmer-derived  $A_V$ , which is typically accurate to around 30%.

Figure 11 plots (purple squares) the IMPZ  $A_V$  values and residuals as a function of Balmer- $A_V$  (multiplied by the Calzetti 2001b factor of 0.44). Note that the IMPZ  $A_V$  values

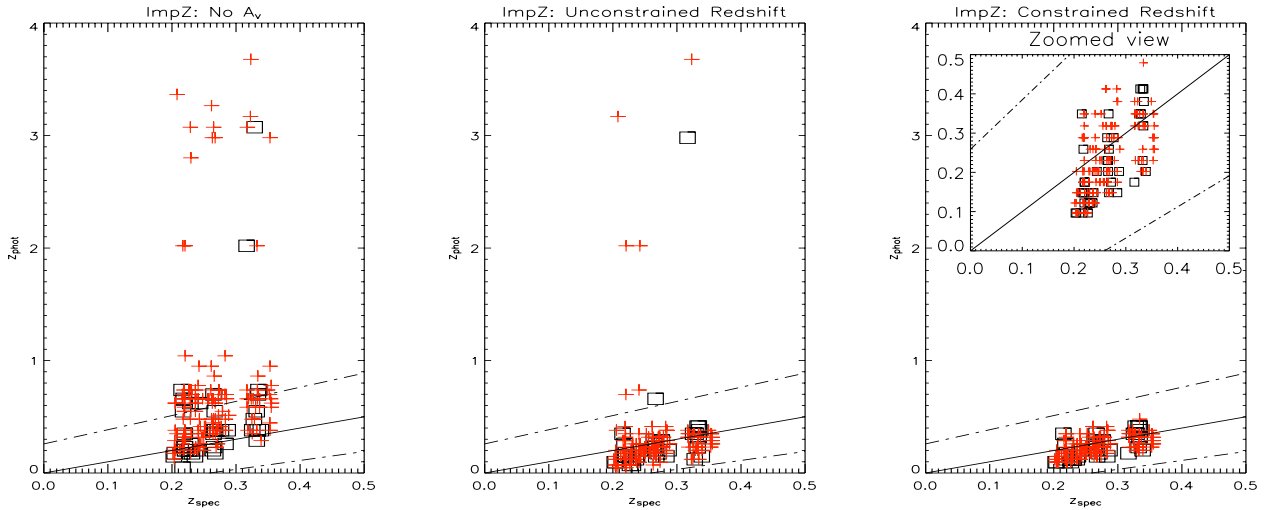


**Figure 7. Photometric redshifts from IMPZ.** Comparison of spectroscopic and IMPZ-derived redshifts for ‘measure’ cases (black squares) and ‘limit’ cases (red crosses): **Left panel** shows results when  $A_V$  freedom is not considered; **middle panel** shows results for unconstrained redshift and  $A_V$  space; **right panel** shows results for redshift space constrained to be within 0.05 in  $\log(1+z_{phot})$  of  $z_{spec}$ , but  $A_V$  unconstrained. Dot-dashed lines denote an accuracy of 0.1 in  $\log(1+z)$ , a typical photometric redshift accuracy.

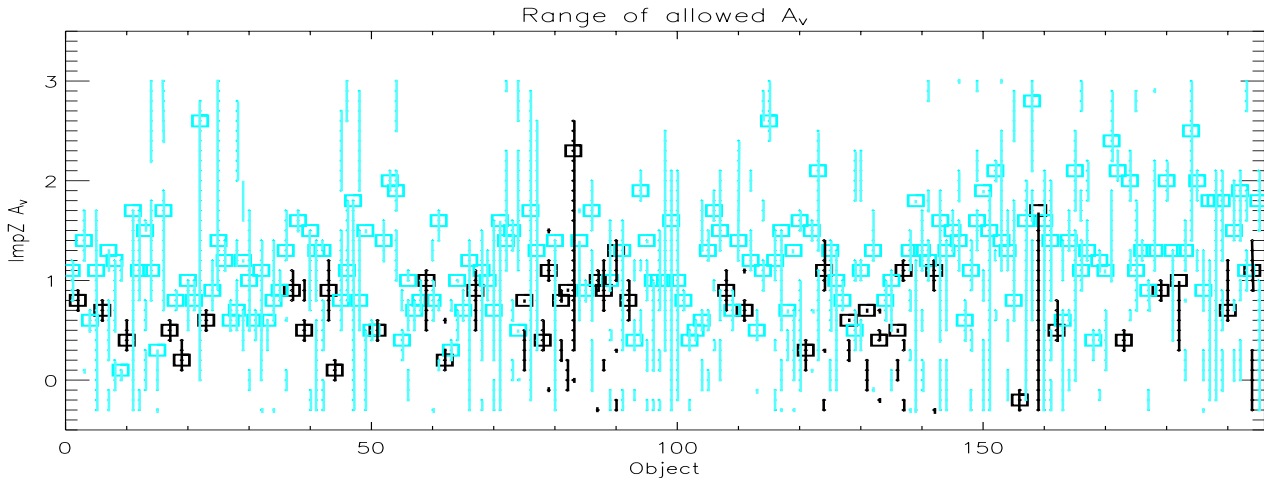


**Figure 8. IMPZ  $A_V$  allowed values.** The range of  $A_V$  parameter space for each source that provides a solution with a reduced  $\chi^2$  within  $\chi^2_{min}+1$  and that is at or near the correct redshift (within 0.05 of  $\log[1+z_{spec}]$ ). ‘Measure’ sources are shown as black lines, ‘limit’ sources as cyan lines. The best  $A_V$  solution value is indicated as a black (‘measure’ case) or cyan (‘limit’ case) square.

have been taken at face-value and have not had an error assigned to them, since we wish to derive an error based on the comparison to the Balmer- $A_V$ 's.

It can be seen that the residuals are smallest for Phot- $A_V$  values of around 0.5 to 1 and that the residuals increase as we move away from this region (to either higher  $A_V$  or lower/negative  $A_V$ ). Hence, the correlation to Balmer-derived  $A_V$  appears to be best for sources of intermediate extinction. It is also clear that none of the sources that were calculated as having negative  $A_V$  based on their Balmer lines obtain similar Phot- $A_V$  values, lending weight to the supposition that the Balmer method has fallen down for these sources due to limitations in the technique. The source with the largest Balmer- $A_V$ , of  $5.15 \pm 0.5$ , is also the source with

the largest residual (of sources with non-negative  $A_V$ ). Being so extinguished, it is likely that this object is quite extreme, so disagreement between the star- and gas-derived extinction measures is to be expected.

Calculating the following statistics:

$$\overline{\Delta A_V} = \sum (Balmer[A_V] - Phot[A_V]) / N \quad (7)$$

and

$$\sigma_{A_V}^2 = \sum (Balmer[A_V] - Phot[A_V])^2 / N \quad (8)$$

and outliers are defined by

$$|\Delta A_V| > 0.5 \quad (9)$$

gives  $\overline{\Delta A_V} = -0.2$ ,  $\sigma_{A_V} = 0.83$  and an outlier fraction,

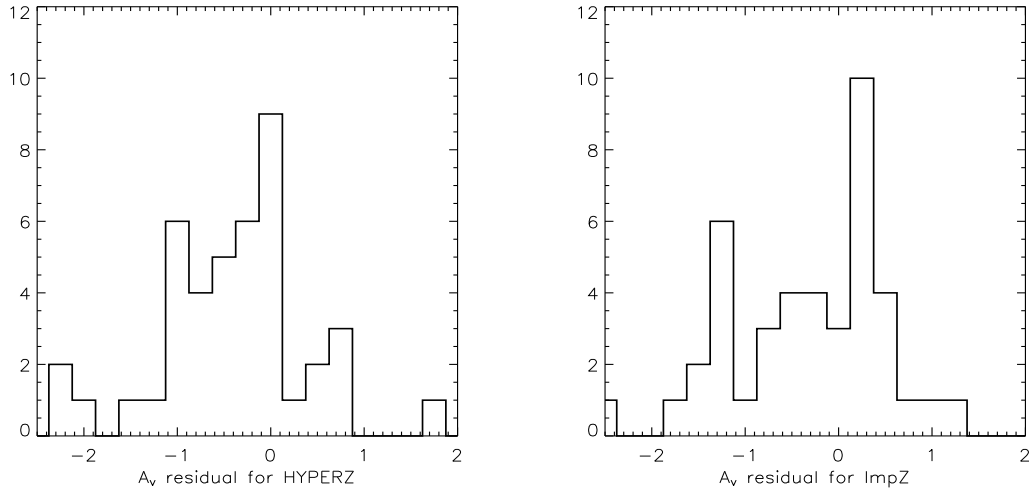


**Figure 10.**  $A_V$  residuals for HYPERZ (left panel) and IMPZ (right panel). The residual is  $(0.44 \cdot \text{Balmer}[A_V] - \text{Phot}[A_V])$ .

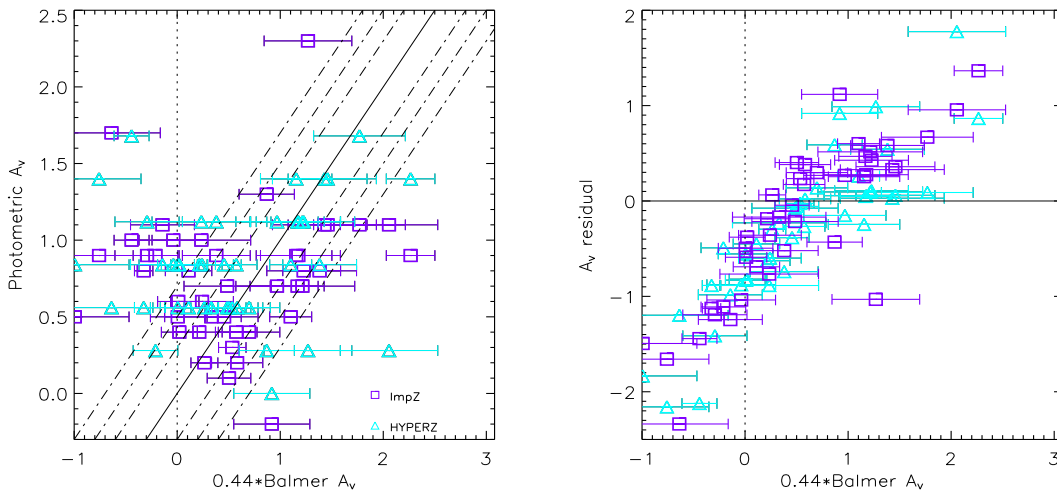


**Figure 11.** **Left:**  $A_V$  results for HYPERZ (cyan triangles) and IMPZ (purple squares). Plot is the  $\text{Balmer}[A_V]$  (multiplied by the Calzetti (2001) factor of 0.44) versus the photometrically-derived  $A_V$ . Dot-dashed lines denote residuals of 0.3, 0.5 and 0.7 in  $A_V$ . Errors are not defined for the  $\text{Phot-}A_V$  values. **Right:**  $A_V$  residuals for HYPERZ (cyan triangles) and IMPZ (purple squares). Plot is  $\text{Balmer-}A_V$  (multiplied by the Calzetti 2001 factor of 0.44) versus the residual  $(0.44 \cdot \text{Balmer}[A_V] - \text{Phot}[A_V])$ .

$\eta$ , of 50 per cent. These results are better than one would infer from the large extinction degeneracies seen in the SSP fitting which were discussed in §4.1. Thus, a relationship between Balmer-derived and photometry-derived extinction measures is obtainable, though not a strong one.

#### 5.4 HYPERZ - comparison to Balmer

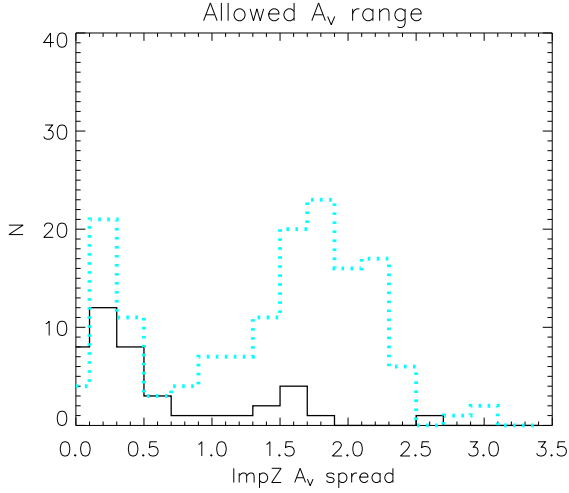
Applying HYPERZ in a ‘best-case’ configuration (constraining the HYPERZ redshift solutions to the spectroscopic values and excluding the elliptical template) gives similar statistics of  $\overline{\Delta A_V} = -0.3$ ,  $\sigma_{A_V} = 0.84$  and an outlier fraction,  $\eta$ , of 50 per cent. The distribution of  $A_V$  residuals for HYPERZ is plotted in Figure 10. As with IMPZ, the distribution is broad but reasonably centred on zero.

Figure 11 plots (cyan triangles) the HYPERZ  $A_V$  values and residuals as a function of  $\text{Balmer-}A_V$  (multiplied by the Calzetti 2001b factor of 0.44). The residuals are again correlated with the  $\text{Balmer-}A_V$ , being smallest for  $\text{Phot-}A_V$  values of around 0.5 to 1, and the negative  $\text{Balmer-}A_V$  sources are again in poor agreement.

Thus, HYPERZ and IMPZ portray a similar correlation to the  $\text{Balmer-}A_V$ , though the agreement is noisy.

#### 5.5 Comparison of IMPZ and HYPERZ

As well as comparing the two photometric redshift code’s extinction outputs to the Balmer-derived values, it is instructive to compare them to one another to see if they tend to



**Figure 9.** Histogram of the width of IMPZ  $A_V$  allowed values. Distribution of the width of  $A_V$  parameter space (defined by the minimum and maximum allowed  $A_V$ ) that lies within  $+1$  of  $\chi^2_{min}$ . ‘Measure’ sources are shown as a black line, ‘limit’ sources as a cyan dotted line.

agree on a similar extinction value for a given source. A plot of IMPZ- $A_V$  versus HYPERZ- $A_V$  is given on Figure 12.

This shows that the two codes are in reasonable agreement about the extinction of a given source. Twenty-five of the forty-two sources (60%) agree within  $< 0.4$  in  $A_V$ , thirty-five sources (83%) agree within  $< 0.5$ . The main difference appears to be for five sources where IMPZ gives a high value of  $A_V > 0.8$  whilst HYPERZ tends to return a smaller  $A_V$  estimate. Two of these sources (this includes object 159 mentioned in §5.2) have Balmer decrements that imply negative, or zero extinction, favouring the HYPERZ result or the interpretation that the sources are problematic. Two others have intermediate Balmer- $A_V$  consistent with either code’s results and one has a larger Balmer- $A_V$  (this is object 83 mentioned in §5.2) thus favouring the IMPZ result.

Calculating similar statistics as when comparing to the Balmer- $A_V$ , comparison between the two codes’  $A_V$  values gives  $\overline{\Delta A_V} = -0.09$ ,  $\sigma_{A_V} = 0.53$  and an outlier fraction,  $\eta$ , of 17 per cent. This internal consistency check between the two codes gives increased confidence in the photometric redshift template-fitting method as a technique to obtain extinction.

### 5.6 The Calzetti ratio

We now consider the empirical ratio of 0.44 introduced by Calzetti (1997) and set out in Eqn. 5. We consider a range of other ratios,  $\gamma$ , so that

$$E(B - V)_s = \gamma E(B - V)_g \quad (10)$$

Varying this ratio from  $0.05 < \gamma < 1$ , a  $\chi^2$  minimisation analysis is carried out in order to find the ratio that gives the best correlation between the Phot- $A_V$  and the Balmer- $A_V$ , weighted by the errors in the Balmer- $A_V$  measurements. The results of this analysis are shown in Figure 13. For both IMPZ and HYPERZ, the lowest reduced  $\chi^2$  is reached for  $\gamma \sim 0.25$ . Based on the change in  $\gamma$  that

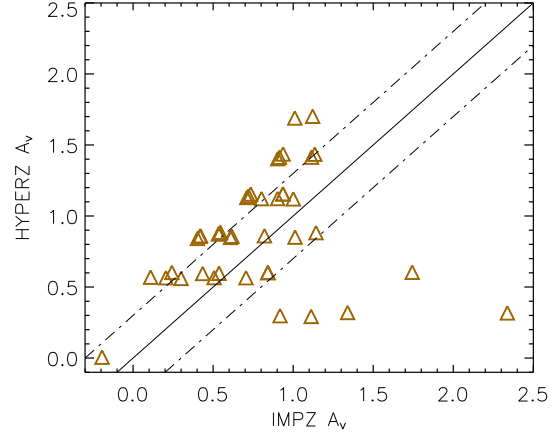


**Figure 12.** Comparison between IMPZ and HYPERZ:  $A_V$  results for IMPZ versus those from HYPERZ. Solid line is exact agreement, dot-dashed lines are residuals of 0.3 in  $A_V$ . Note that for plotting purposes the values have been randomly altered by up to 0.02 in the x and y directions in order to separate points with the same/very similar values.

**Table 4.** Statistical results for the different comparisons between Balmer- $A_V$  and Phot- $A_V$ .

	$\overline{\Delta A_V}$	$\sigma_{A_V}$	outlier fraction, $\eta$
IMPZ, $\gamma=0.44$	-0.2	0.83	50%
HYPERZ, $\gamma=0.44$	-0.3	0.84	50%
IMPZ, $\gamma=0.25$	-0.4	0.72	38%
HYPERZ, $\gamma=0.25$	-0.5	0.76	57%
IMPZ/HYPERZ comparison	-0.09	0.53	17%

increases the reduced  $\chi^2$  by one, the  $1\sigma$  error on this value is  $\gamma = 0.25 \pm 0.25$  for IMPZ and  $\gamma = 0.25 \pm 0.1$  for HYPERZ.

The resulting statistical measures,  $\sigma_{A_V}$  and the outlier fraction,  $\eta$ , are also plotted as a function of  $\gamma$  for the IMPZ and HYPERZ results (Figure 14). The left panel shows how the *rms* in the residual,  $\sigma_{A_V}$ , varies with  $\gamma$ . A clear minimum is seen at  $\gamma \sim 0.15$  to  $0.35$  for IMPZ results, and at around 0.2 to 0.4 for HYPERZ. A similar minimum is seen in the range  $\gamma \sim 0.2$  to  $0.35$  for IMPZ results when the outlier fraction,  $\eta$ , is plotted against  $\gamma$  in the right-hand panel. For HYPERZ, the minimum is at around  $\gamma \sim 0.3$  to 0.45.

This analysis suggests that for this sample, the Calzetti ratio of 0.44 is a reasonable choice for  $\gamma$  within the accuracy of the method, though a value of  $\sim 0.25$  is preferred. A choice of  $\gamma=0.25$  gives the following statistics:

For IMPZ;  $\overline{\Delta A_V} = -0.4$ ,  $\sigma_{A_V} = 0.72$  and an outlier fraction,  $\eta$ , of 38 per cent.

For HYPERZ;  $\overline{\Delta A_V} = -0.5$ ,  $\sigma_{A_V} = 0.76$ ,  $\eta$ , of 57 per cent.

As before, the distribution of  $A_V$  residuals is plotted (Figure 15). It can be seen that the distribution is more peaked, though offset from zero.

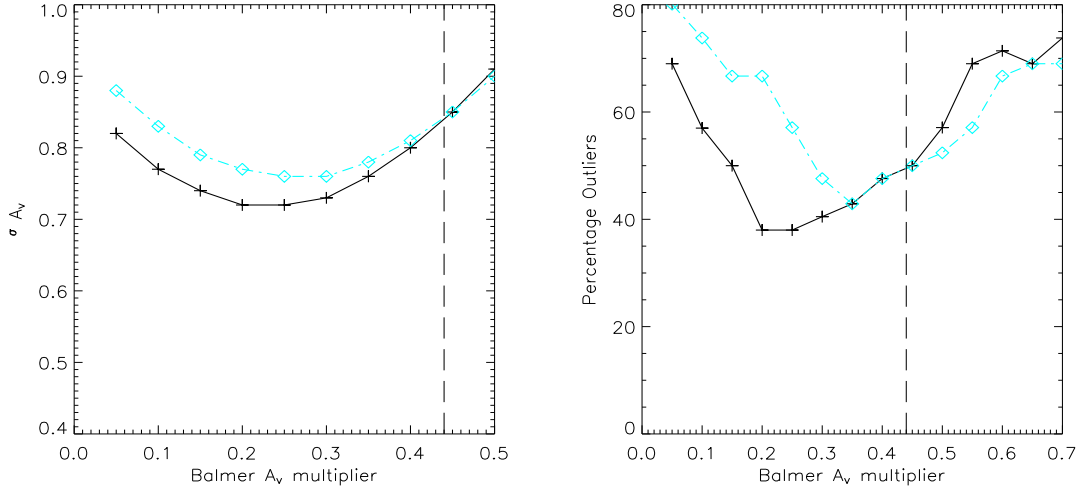


**Figure 14.** **Left panel:**  $\sigma_{A_V}$  for IMPZ (solid line with crosses) and HYPERZ (dot-dashed blue line, diamonds) as a function of  $\gamma$ , the chosen ratio between photometrically-derived and Balmer ratio-derived extinction measures. The Calzetti value of  $\gamma = 0.44$  is indicated as a long-dashed line. **Right panel:** Percentage outliers for IMPZ (solid line with crosses) and HYPERZ (dot-dashed blue line, diamonds) as a function of  $\gamma$ , the chosen ratio between photometrically-derived and Balmer ratio-derived extinction measures. The Calzetti value of  $\gamma = 0.44$  is indicated as a long-dashed line.

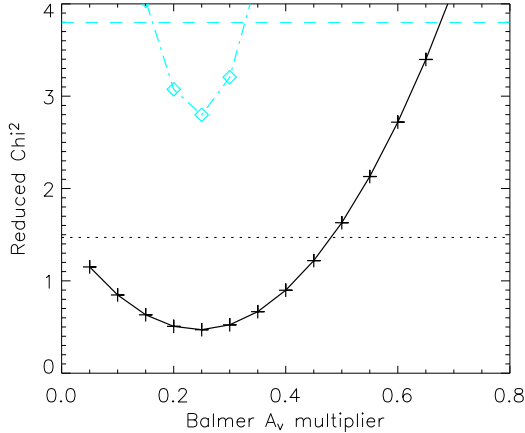


**Figure 13.**  $\chi^2$  analysis. The reduced  $\chi^2$  for IMPZ (solid line with crosses) and HYPERZ (dot-dashed line, diamonds) as a function of  $\gamma$ , the chosen ratio between photometrically-derived and Balmer ratio-derived extinction measures. The  $\chi^2$  values that are 1 above the minimum in the two distributions are indicated by horizontal lines (IMPZ, dotted; HYPERZ, dashed).

Figure 16 plots the Phot- $A_V$  values and residuals as a function of Balmer- $A_V$  (multiplied by  $\gamma=0.25$ ). It can be seen that for lower Balmer- $A_V$ , the Balmer- $A_V$  tends to underestimate the extinction in comparison to the Phot- $A_V$  value. If the negative Balmer- $A_V$  are excluded, then the remaining sources with positive Balmer- $A_V$  do tend to follow the line denoting agreement, albeit with large scatter.

In Figure 17 the sources with only a lower limit on their Balmer-derived extinction (that is, a minimum  $3\sigma$  H $\alpha$  detection but only a limit on the H $\beta$  line detection) are plotted in comparison to the extinction as derived from the pho-

tometric redshift codes. Here, no ratio  $\gamma$  is applied to the Balmer  $A_V$ . Instead straight lines indicating different ratios are overplotted. Since these are lower limits, sources need to lie on, or to the left of a line to imply consistency with that chosen ratio. It can be seen that these lower limit sources are more consistent with lower values of  $\gamma$ . Of the 153 such sources, 146 (95%) are consistent with the  $\gamma=0.25$  line when considering IMPZ solutions (purple squares), but only 130 (85%) are consistent when considering the HYPERZ solutions (cyan triangles).

## 6 DISCUSSIONS AND CONCLUSIONS

A number of redshift codes routinely output an  $A_V$  value in addition to the best-fitting redshift, but little has been done to investigate the reliability and/or accuracy of such extinction measures. The main reason for this lies in the aim of such codes - they have been developed and optimised in order to derive *redshifts*. However, as the field of photometric redshift derivation matures, it is useful to consider some of the other parameters that redshift solutions output.

In this paper we have asked the question ‘Can a photometric redshift code reliably determine dust extinction?’. The short answer would be: ‘Not to a great accuracy’.

Using a sample with extinctions derived from Balmer flux-ratios the  $A_V$  values produced by two photometric redshift codes, IMPZ and HYPERZ, have been compared to the Balmer- $A_V$  values.

First, it was demonstrated that the inclusion of  $A_V$  was crucial in order to obtain photometric redshifts of high accuracy and reliability, such that 95% of the IMPZ results agreed with the spectroscopic redshifts to better than 0.1 in  $\log[1+z]$ . Without the inclusion of  $A_V$  freedom, there was a systematic and incorrect offset to higher photometric

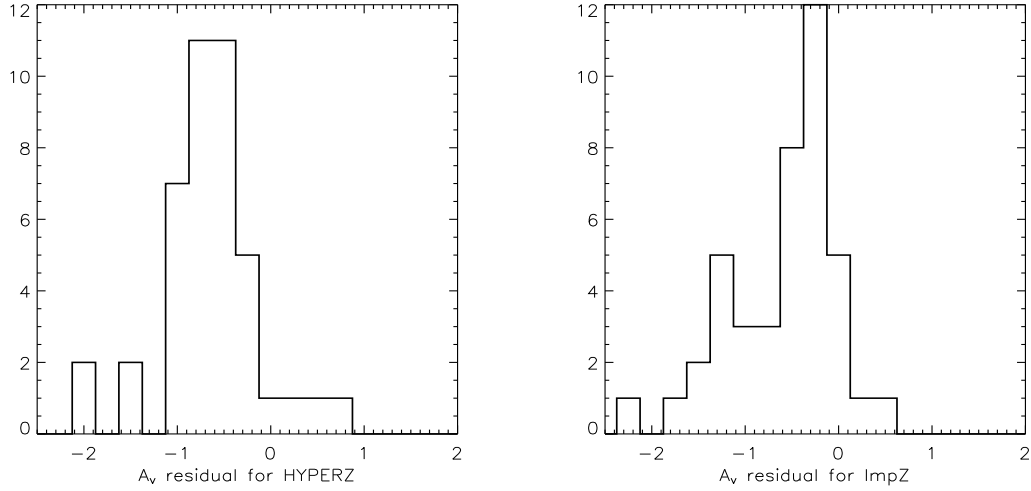


**Figure 15.**  $A_V$  residuals for HYPERZ (left panel) and IMPZ (right panel) with  $\gamma=0.25$ . The residual is now  $(0.25*\text{Balmer}[A_V]-\text{Phot}[A_V])$ .

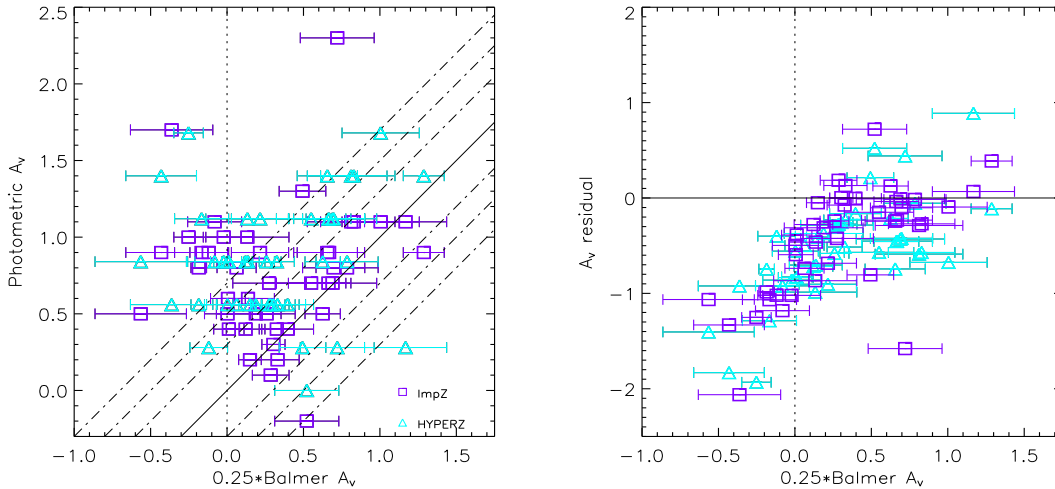


**Figure 16.** **Left:**  $A_V$  results for HYPERZ (cyan triangles) and IMPZ (purple squares). Plot is the Balmer $[A_V]$  (multiplied by  $\gamma = 0.25$ ) versus the photometrically-derived  $A_V$ . Dot-dashed lines denote residuals of 0.3, 0.5 and 0.7 in  $A_V$ . Errors are not defined for the Phot- $A_V$  values. **Right:**  $A_V$  residuals for HYPERZ (cyan triangles) and IMPZ (purple squares). Plot is Balmer- $A_V$  (multiplied by  $\gamma = 0.25$ ) versus the residual  $(0.25*\text{Balmer}[A_V]-\text{Phot}[A_V])$ .

redshifts with many more incorrect redshift solutions. The existence of some negative  $A_V$  solutions may be indicative of the need for a bluer template in the template set, or for the inclusion of some additional free parameter in the fits. As the most important feature for template-fitted photometric redshifts is the location and identification of ‘breaks’ in the SED, the inclusion of  $A_V$  freedom can be seen, at first-order, as a modifier of the template SED’s slope without having a strong effect on the breaks themselves. Hence a similar improvement may be achievable via a ‘tilting’ parameter or similar which would act to alter the slope of the template SEDs. Since addition of dust extinction has a physical basis, however, this is a preferable parameter, as long as we can demonstrate that there is some correlation between

the best-fitting phot- $A_V$  and the actual (or in this case, that measured via the Balmer ratio) dust extinction of the source. Thus, once the ability to derive good redshifts for the sample had been demonstrated a comparison between the phot- $A_V$  and Balmer- $A_V$  was carried out:

The correlation between the Phot- $A_V$  and the Balmer- $A_V$  was similar for both codes, but was both noisy and not particularly strong. Based on direct comparison between the two codes, and investigations into the  $\chi^2$  solution space, a good part of this noise is derived from the inherent lack of precision the Phot- $A_V$  solution has (perhaps 0.3 in  $A_V$  say), no doubt since it is based on only five photometric measurements. Additional noise arises from the precision of the Balmer- $A_V$ , typically accurate to perhaps 30%, which

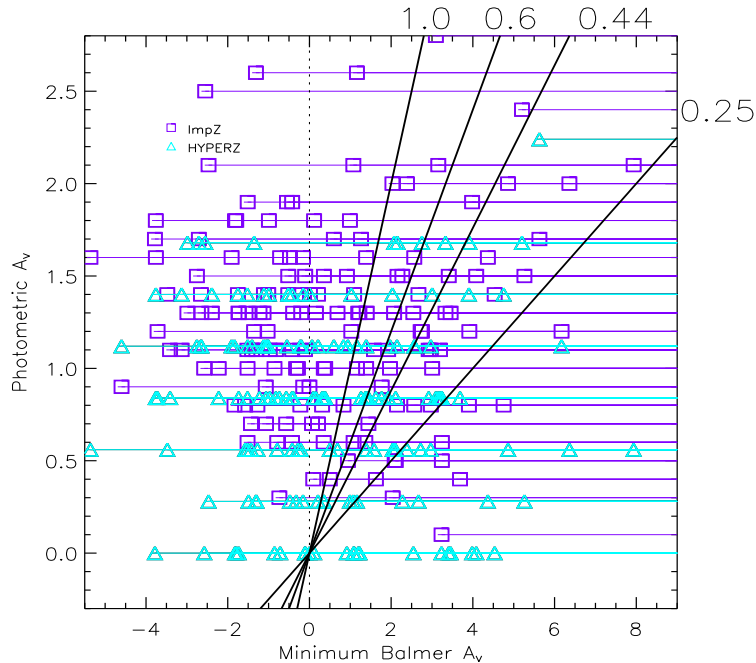


**Figure 17. ‘Limit’ cases:**  $A_V$  results for HYPERZ (cyan triangles) and IMPZ (purple squares). Plot is the Balmer-derived  $A_V$  ‘limits’ versus the photometrically-derived  $A_V$ . Solid black lines denote  $\gamma$  values of 0.25, 0.44, 0.6 and 1.0 for the conversion factor relating Balmer- $A_V$  and Phot- $A_V$ . Sources need to lie on, or to the left of a line to imply consistency with that chosen ratio.

is due to the resolution of the spectrographic data. Given these errors, the correlation seen was in fact quite good.

The correlation was improved somewhat when the empirical value of  $\gamma = 0.44$ , the ratio between gas- and star-derived extinction, as determined by Calzetti (2001b), was allowed to vary. From least-squares-fitting the minimum in the reduced  $\chi^2$  distribution was found for  $\gamma \sim 0.25 \pm 0.2$ .

The Calzetti ratio of 0.44 means that there is around a factor two difference in reddening such that the ionised gas (as measured by the Balmer decrement) is twice as reddened as the stellar continua (as measured by the photometry) (e.g Fanelli et al. 1988; Calzetti et al. 1994). This implies that the covering factor of the dust is larger for the gas than for the stars, which can be explained by the fact that the ionising stars are short-lived and so for their lifetime remain relatively close to their (dusty) birthplace, whilst the majority of stars, contributing to the galaxy’s overall optical luminosity are longer-lived and can migrate away from their dusty origins.

For the sample of galaxies in this paper, this factor two difference in covering factor implied by the Calzetti ratio is found to be plausible, given the errors of the method. The sample has a some preference for an increased covering factor which would imply they are undergoing more rapid, ‘bursty’ star formation than the galaxies Calzetti used in her derivation. Perhaps more importantly, the results demonstrate the pitfalls of assuming that star- and gas-based extinction measures will give the same dust extinction given some conversion factor. Thus, correlation to Balmer-derived values are modulo the uncertainty in comparing star- and gas-based extinction measures.

However the results presented here show that, given certain considerations, there is potential in the application of photometric codes to reliably derive an extinction measure, though the precision is currently low. It is expected that the ability of photometric redshift codes to determine extinction will improve with the availability of more photometric bands (here, there are five wide band filters between 3,000-9,000Å). A sample with a combination of wide and narrow-band filters, with good wavelength coverage and range (in particular, extension to near-IR) will break many of the degeneracies and allow the codes to accurately differentiate between different possible fits.

The results also show that it is important to note that this will be a measure of the star-based extinction, and will not necessarily be well correlated with the extinction to the ionised regions of a galaxy.

## 7 ACKNOWLEDGEMENTS

We would like to thank Michael Rowan-Robinson for discussions on the nature of dust extinction and SED templates. The referee provided astute suggestions and comments on this work and we extend our thanks. We also thank those responsible for the CNOC2 survey whose data we have used here.

## REFERENCES

Adelberger K., Steidel C., 2000, ApJ, 544, 218

- Babbedge T. S. R., Rowan-Robinson M., Gonzales-Solares E. A., Polletta M., Berta S., Pérez-Fournon I., Oliver S., Salaman M., Irwin M., (**B04**), 2004, MNRAS, 353, 654
- Balogh M., 1999, Ph.D. Thesis
- Balogh M., Bower, R. G., Smail, I., Ziegler, B. L., Davies, R. L., Gaztelu, A., Fritz, A., 2002, MNRAS, 337, 256
- Berta S., Fritz J., Franceschini A., Bressan A., Lonsdale C., 2004, AAP, 418, 913
- Bohlin R., Jenkins E., Spitzer L., York D., Hill J., Savage B., Snow T., 1983, ApJS, 51, 277
- Bolzonella M., Miralles J.-M., Pelló R., 2000, AAP, 363, 476
- Bressan A., Granato G., Silva L., 1998, AAP, 332, 135
- Calzetti D., 1997, astro-ph/9706121
- Calzetti D., 2001a, PASP, 113, 1449
- Calzetti D., 2001b, New Astronomy Review, 45, 601
- Calzetti D., Armus L., Bohlin R., Kinney A., Koornneef J., Storchi-Bergmann T., 2000, ApJ, 533, 682
- Calzetti D., Heckman T., 1999, ApJ, 519, 27
- Calzetti D., Kinney A., Storchi-Bergmann T., 1994, ApJ, 429, 582
- Calzetti D., Kinney A., Storchi-Bergmann T., 1996, ApJ, 458, 132
- Calzetti D., Kinney A., Storchi-Bergmann T., Panagia N., 1993, Bulletin of the American Astronomical Society, 25, 841
- Cardelli J., Clayton G., Mathis J., 1989, ApJ, 345, 245
- Carlberg R., Yee H., Morris S., Lin H., Hall P., Patton D., Sawicki M., Shepherd C., 2000, ApJ, 542, 57
- Crampton D., et al. 1992, in M.H Ulrich ed., Proc. ESO Conf. on Progress in Telescop and Instrumentation Technologies MOS/SIS Project
- Dressler A., Shectman S.A., 1987, AJ, 94, 899
- Fanelli M., O'Connell R., Thuan T., 1988, ApJ, 334, 665
- Ferland G., Korista K., Verner D., Ferguson J., Kingdon J., Verner E., 1998, PASP, 110, 761
- Hauser M., Arendt R., Kelsall T., Dwek E., Odegard N., Weiland J., Freudenreich H., Reach W., Silverberg R., Moseley S., Pei Y., Lubin P., Mather J., Shafer R., Smoot G., Weiss R., Wilkinson D., Wright E., 1998, ApJ, 508, 25
- Hopkins, A. M., Miller, C. J., Nichol, R. C., Connolly, A. J., Bernardi, M., Gómez, P. L., Goto, T., Tremonti, C. A., Brinkmann, J., Ivezić, Ž., Lamb, D. Q., 2003, ApJ, 599, 971
- Kennicutt R., 1992, ApJ, 388, 310
- Kennicutt R.C., Kent S.M., 1983, AJ, 88, 1094
- Kewley L., Geller M., Jansen R., Dopita M., 2002, AJ, 124, 3135
- Kurucz R., 1993, ATLAS9 Stellar Atmosphere Programs and 2 km/s grid. Kurucz CD-ROM No.13. Cambridge, Mass. Smithsonian Astrophysical Observatory, 1993., 13
- Madau P., Ferguson H., Dickinson M., Giavalisco M., Steidel C., Fruchter A., 1996, MNRAS, 283, 1388
- Massarotti M., Iovino A., Buzzoni A., 2001, AAP, 368, 74
- Meurer G., Heckman T., Calzetti D., 1999, ApJ, 521, 64
- Miller N.A., Owen F.N., 2002, AJ, 124, 2453
- Osterbrock D., 1989, Astrophysics of Gaseous Nebulae and Active Galactic Nuclei. Mill Valley CA: University Science Books
- Pettini M., Kellogg M., Steidel C., Dickinson M., Adelberger K., Giavalisco M., 1998, ApJ, 508, 539
- Pickles A., 1998, PASP, 110, 863
- Puget J. L., Abergel A., Bernard J. P., Boulanger F., Burton W. B., Desert F. X., Hartmann D., 1996, AAP, 308, L5
- Rowan-Robinson M., (**RR03**), 2003, MNRAS, 344, 13
- Rowan-Robinson M., Mann R., Oliver S., Efstathiou A., Eaton N., Goldschmidt P., Mobasher B., Serjeant S., et al. 1997, MNRAS, 289, 490
- Savage B., Mathis J., 1979, ARA&A, 17, 73
- Shepherd C., Carlberg R., Yee H., Morris S., Lin H., Sawicki M., Hall P., Patton D., 2001, ApJ, 560, 72
- Tody D., 1993, in ASP Conf. Ser. 52: Astronomical Data Analysis Software and Systems II IRAF in the Nineties. p. 173
- Westera P., Cuisinier F., Telles E., Kehrig C., 2004, AAP, 423, 133
- Yee H., Morris S., Lin H., Carlberg R., Hall P., Sawicki M., Patton D., Wirth G., Ellingson E., Shepherd C., 2000, ApJS, 129, 475